Article

Structural Transformations and Adsorption of Fuel-Related Gases of a Structurally Responsive Nickel Phosphonate Metal#Organic Framework, Ni-STA-12

Stuart R. Miller, Gordon M. Pearce, Paul A. Wright, Francesca Bonino, Sachin Chavan, Silvia Bordiga, Irene Margiolaki, Nathalie Guillou, Ge#rard Fe#rey, Sandrine Bourrelly, and Philip L. Llewellyn

J. Am. Chem. Soc., **2008**, 130 (47), 15967-15981 • DOI: 10.1021/ja804936z • Publication Date (Web): 30 October 2008

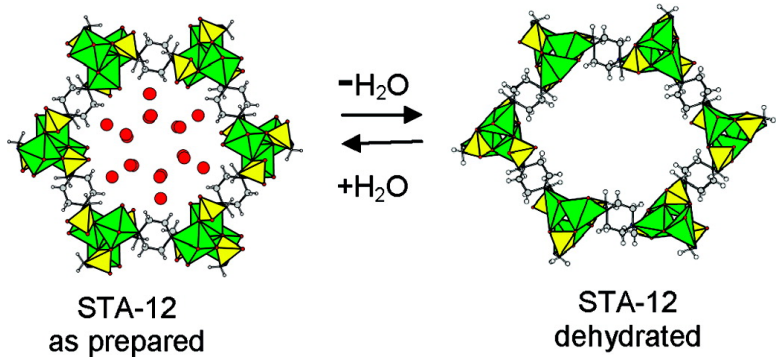

More About This Article

Additional resources and features associated with this article are available within the HTML version:

- Supporting Information
- Links to the 1 articles that cite this article, as of the time of this article download
- Access to high resolution figures
- Links to articles and content related to this article
- Copyright permission to reproduce figures and/or text from this article

View the Full Text HTML

J|A|C|S
ARTICLES

Published on Web 10/30/2008

Structural Transformations and Adsorption of Fuel-Related Gases of a Structurally Responsive Nickel Phosphonate Metal−Organic Framework, Ni-STA-12

Stuart R. Miller,[†] Gordon M. Pearce,[†] Paul A. Wright,*[,†] Francesca Bonino,[‡] Sachin Chavan,[‡] Silvia Bordiga,[‡] Irene Margiolaki,[§] Nathalie Guillou,[||] Gérard Férey,[||] Sandrine Bourrelly,[⊥] and Philip L. Llewellyn[⊥]

School of Chemistry, University of St Andrews, Purdie Building, North Haugh, St Andrews, Fife, KY16 9ST U.K., Department of Inorganic, Physical and Materials Chemistry and NIS Centre of Excellence and INSTM Centro di Riferimento, University of Turin, Via P Giuria 7, I-10125 Turin, Italy, European Synchrotron Radiation Facility, F-38043 Grenoble, France, Institut Lavoisier, Université de Versailles St-Quentin en Yvelines—CNRS, UMR 8180, 45, Avenue des Etats-Unis, 78035 Versailles cedex, France, and Laboratoire Chimie Provence, Universités d'Aix-Marseille I, II & III−CNRS, UMR 6264, Centre de Saint Jérôme, 13397 Marseille cedex 20, France

Received June 27, 2008; E-mail: paw2@st-andrews.ac.uk

Abstract: The structure of the nickel *N,N′*-piperazinebismethylenephosphonate, Ni-STA-12 (St. Andrews porous material-12), has been determined in the hydrated ($Ni_2L\cdot 8H_2O$, L = $O_3PCH_2NC_4H_8NCH_2PO_3$), partially dehydrated ($Ni_2L\cdot 2H_2O$), and fully dehydrated (Ni_2L) forms from high-resolution synchrotron X-ray powder diffraction. The framework structures of $Ni_2L\cdot 8H_2O$ and $Ni_2L\cdot 2H_2O$ are almost identical ($R\bar{3}$, a = 27.8342(1) Å, c = 6.2421(2) Å; $R\bar{3}$, a = 27.9144(1) Å, c = 6.1655(2) Å) with additional physisorbed water of the as-prepared Ni-STA-12 present in an ordered hydrogen-bonded network in the channels. *Ab initio* structure solution of the fully dehydrated solid indicates it has changed symmetry to triclinic ($P\bar{1}$, a = 6.03475(5) Å, b = 14.9157(2) Å, c = 16.1572(2) Å, α = 112.5721(7)°, β = 95.7025(11)°, γ = 96.4950(11)°) as a result of a topotactic structural rearrangement. The fully dehydrated solid possesses permanent porosity with elliptical channels 8 Å × 9 Å in free diameter. The structural change results from the loss of water coordinated to the nickel cations, so that the nickel coordination changes from edge-sharing octahedral NiO_5N to edge- and corner-sharing five-fold NiO_4N. During this change, two out of three phosphonate groups rotate to become fully coordinated to nickel cations, leaving the remainder of the phosphonate groups coordinated to nickel cations by two oxygen atoms and with a P═O bond projecting into the channels. This transformation, which is completely reversible, causes substantial changes in both vibrational and electronic properties as shown by IR, Raman, and UV−visible spectroscopies. Complementary adsorption, calorimetric, and infrared studies of the probe adsorbates H_2, CO, and CO_2 reveal the presence of several distinct adsorption sites in the solid, which are attributed to their interactions with nickel cations which are weak Lewis acid sites, as well as with P═O groups that project into the pores. At 304 K, the adsorption isotherms and enthalpies of adsorption on dehydrated Ni-STA-12 have been measured for CO_2 and CH_4: Ni-STA-12 gives adsorption uptakes of CO_2 of 2.5 mmol g^{-1} at 1 bar, an uptake *ca.* 10 times that of CH_4.

1. Introduction

Hybrid organic−inorganic microporous solids are of increasing importance in solid-state and materials chemistry. In the past 15 years there has been a rapid expansion of their range, and metal carboxylates have received particular recent attention. Many microporous, three-dimensionally connected framework structures have been discovered that are thermally stable to 700 K, have pores up to *ca.* 20 Å in free diameter, and have remarkable adsorption properties, including very high surface areas, structural flexibility, and uncoordinated metal adsorption sites.[1,2] HKUST-1,[3] MOF-5,[4] and MIL-100[5] are among the best known examples of such metal−organic frameworks, or MOFs, in which metallocentric nodes and di-, tri-, or tetracarboxylic acids are combined in a modular way. Although metal carboxylates are now the best known of the microporous hybrid solids,

[†] University of St Andrews.
[‡] University of Turin.
[§] European Synchrotron Radiation Facility.
[||] Université de Versailles St-Quentin en Yvelines.
[⊥] Universités d'Aix-Marseille I, II & III.

(1) Prestipino, C.; Regli, L.; Vitillo, J. G.; Bonino, F.; Damin, A.; Lamberti, C.; Zecchina, A.; Solari, P. L.; Kongshaug, K. O.; Bordiga, S. *Chem. Mater.* **2006**, *18*, 1337–1346.
(2) Bonino, F.; Chavan, S.; Vitillo, J. G.; Groppo, E.; Agostini, G.; Lamberti, C.; Dietzel, P. D. C.; Prestipino, C.; Bordiga, S. *Chem. Mater.* **2008**, *20*, 4957–4968.
(3) Chui, S. S. Y.; Charmant, J. P. H.; Orpen, A. G.; Williams, I. D. *Science* **1999**, *283*, 1148–1150.
(4) Li, H.; Eddaoudi, M.; O'Keeffe, M.; Yaghi, O. M. *Nature* **1999**, *402*, 276–279.
(5) Férey, G.; Mellot-Draznieks, C.; Serre, C.; Millange, F. *Acc. Chem. Res.* **2005**, *38*, 217–225.

there are many other families of porous MOFs, including those based on amines (such as the zeolitic imidazolates[6,7]), mixed amine−carboxylates,[8−10] and amino acids.[11] A review of the current state of the art is given by Férey.[12]

Metal phosphonates also occupy an important place among the families of porous organic−inorganic hybrids.[13−16] As is the case with carboxylates, there is a rich variety of phosphonate building units that can be used as reagents (as acids or esters, for example) that are either commercially available or readily synthesized, and like carboxylates, phosphonates form strong bonds with a range of metal cations when they can bind through one, two, or three of these oxygen atoms per phosphonate group. Furthermore, the O_3P-C bond is stable to elevated temperatures. As a result, it is possible to prepare phosphonate frameworks stable to high temperatures that would be competitive with metal carboxylate MOFs in applications.

Whereas many highly porous metal carboxylates and amine MOFs have been prepared, attempts to generate three-dimensionally crystalline microporous analogues using di-, tri-, or tetraphosphonate linkers have only relatively recently begun to give structures of interest as adsorbents. Important organically pillared metal phosphonates with porosity have been prepared in this size domain,[13−15] but these do not have perfect long-range order, and their pore structure is not defined exactly by their crystal structure. If grouped according to ligand type, microporous metal phosphonates prepared with the *N*,*N*′-piperazinebismethylenephosphonate ligand ($O_3PCH_2NC_4H_8NCH_2PO_3$, denoted L in this paper) are of particular interest.[17−21] This remarkably flexible ligand has been shown to be able to cross-link one-dimensional (1-D) inorganic chains by binding via two or three oxygen atoms per phosphonate group, and in some cases also via the nitrogen of the piperazine ring. The first open-framework solids of this type were of the formula MH_2L (M^{II} = Mn, Co), where inorganic chains containing tetrahedrally coordinated metal cations are linked by the bisphosphonate ligands, protonated on the nitrogen atoms, to give 1-D narrow channels containing water molecules.[17] The same ligand gives the porous solids labeled MIL-91(Al,Ti), where the inorganic species make up chains, this time with the metals in octahedral coordination, and these chains are cross-linked by the ligands, leaving channels with free dimensions (perpendicular to the channel axis) of 4 Å, able to adsorb small gas molecules with pore volumes of up to 0.19 $cm^3\ g^{-1}$.[20]

The porous divalent metal phosphonates that we prepared with this ligand, with composition $M_2L\cdot nH_2O$ (n = 7−8; M = Fe, Co, Ni; STA-12 = St Andrews nanoporous material-12), are remarkable in that they are the first fully crystalline metal phosphonate MOFs with pores approaching 1 nm.[21] Other microporous metal phosphonates with well-defined crystal structures are known, but these only have pores with free diameters up to *ca*. 6 Å.[16,20−24] Furthermore, the specific pore volume measured for the dehydrated form of this solid (measured in the range 0.17−0.21 $cm^3\ g^{-1}$) is similar to the highest values previously reported for other crystalline metal phosphonates (such as the less thermally stable MIL-91[20]) and approaches values observed for large-pore zeolites (zeolite-β, 0.22 $cm^3\ g^{-1}$). Studies of the nickel version of STA-12 revealed a highly porous solid which, when fully hydrated, contains channels *ca*. 1 nm in diameter, filled with water molecules (Figure 1). The framework of the as-prepared solid is built from helical chains of edge-sharing NiO_5N octahedra, linked into a honeycomb arrangement via the ligands. A key structural feature of this solid, which imparts thermal stability up to 650 K, is the coordination of the ligand to the metal atoms of the inorganic chain via phosphonate oxygen atoms and a piperazine ring nitrogen atom.

The structure of Ni-STA-12 at different levels of hydration has been determined by high-resolution synchrotron powder X-ray diffraction (XRD) combined with IR, Raman, and UV−visible spectroscopies. The latter have been used in order to follow the changes in the local structure of the framework during reversible dehydration and rehydration. The mechanism of adsorption on the fully dehydrated sample has been examined by IR measurements upon uptake of H_2 and CO at low temperature and CO_2, CH_3OH, and CD_3CN at room temperature. These molecules have been shown to be excellent probes of adsorption sites.[25−28] Finally, we have investigated the adsorption properties at room temperature of dehydrated Ni-STA-12 for the fuel-related gases CO_2 and CH_4 and related them to the structure of the adsorbent.

The picture that emerges is of a hydrated large-pore solid that shows reversible dehydration leading to significant structural rearrangement, with a symmetry change from rhombohedral to triclinic but only a small associated reduction in the pore size. The channels of the fully hydrated material contain water that is ordered at low temperature. During dehydration, substantial

(6) Huang, X. C.; Lin, Y. Y.; Zhang, J. P.; Chen, X. M. *Angew. Chem., Int. Ed.* **2006**, *45*, 1557–1559.
(7) Park, K. S.; Ni, Z.; Côté, A. P.; Choi, J. Y.; Huang, R. D.; Uribe-Romo, F. J.; Chae, H. K.; O'Keeffe, M.; Yaghi, O. M. *Proc. Natl. Acad. Sci. U.S.A.* **2006**, *103*, 10186–10191.
(8) Dybtsev, D. N.; Chun, H.; Kim, K. *Angew. Chem., Int. Ed.* **2004**, *43*, 5033–5036.
(9) Matsuda, R.; Kituara, R.; Kitagawa, S.; Kubota, Y.; Belosludov, R. V.; Kobayashi, T. C.; Sakamoto, H.; Chiba, T.; Takata, M.; Kawazoe, Y.; Mita, Y. *Nature* **2005**, *436*, 238–241.
(10) Matsuda, R.; Kitaura, R.; Kitagawa, S.; Kubota, Y.; Kobayashi, T.C.; Horike, S.; Takata, M. *J. Am. Chem. Soc.* **2004**, *126*, 14063–14070.
(11) Vaidhyanathan, R.; Bradshaw, D.; Rebilly, J. N.; Barrio, J. P.; Gould, J. A.; Berry, N. G.; Rosseinsky, M. J. *Angew. Chem., Int. Ed.* **2006**, *45*, 6495–6499.
(12) Férey, G. *Chem. Soc. Rev.* **2008**, *87*, 191–214.
(13) Alberti, G.; Costantino, U.; Marmottini, F.; Vivani, R.; Zappelli, P. *Angew. Chem., Int. Ed. Engl.* **1993**, *32*, 1357–1359.
(14) Clearfield, A.; Wang, Z. K. *J. Chem. Soc., Dalton Trans.* **2002**, 2937–2947.
(15) Gomez-Alcantara, M. D.; Cabeza, A.; Moreno-Real, M. A. G.; Clearfield, A. *Micropor. Mesopor. Mater.* **2006**, *88*, 293–303.
(16) Maeda, K. *Micropor. Mesopor. Mater.* **2004**, *73*, 47–55.
(17) La Duca, R.; Rose, D.; DeBord, J. R. D.; Haushalter, R. C.; O'Connor, C. J.; Zubieta, J. *J. Solid State Chem.* **1996**, *123*, 408–412.
(18) Groves, J. A.; Wright, P. A.; Lightfoot, P. *Inorg. Chem.* **2005**, *44*, 1736–1739.
(19) Groves, J. A.; Stephens, N. F.; Wright, P. A.; Lightfoot, P. *Solid State Sci.* **2006**, *8*, 397–403.
(20) Serre, C.; Groves, J. A.; Lightfoot, P.; Slawin, A. M. Z.; Wright, P. A.; Stock, N.; Bein, T.; Haouas, M.; Taulelle, F.; Férey, G. *Chem. Mater.* **2006**, *18*, 1451–1457.
(21) Groves, J. A.; Miller, S. R.; Warrender, S. J.; Mellot-Draznieks, C.; Lightfoot, P.; Wright, P. A. *Chem. Commun.* **2006**, 3305–3307.
(22) Liang, J.; Shimizu, G. K. H. *Inorg. Chem.* **2007**, *46*, 10449–10451.
(23) Taylor, J. M.; Mahmoudkhani, A. H.; Shimizu, G. K. H. *Angew. Chem., Int. Ed.* **2007**, *46*, 795–798.
(24) Shi, F. N.; Cunha-Silva, L.; Ferreira, R. A. S.; Mafra, L.; Trindade, T.; Carlos, L. D.; Paz, F. A. A.; Rocha, J. *J. Am. Chem. Soc.* **2008**, *130*, 150–167.
(25) Lamberti, C.; Groppo, E.; Spoto, G.; Bordiga, S.; Zecchina, A. *Adv. Catal.* **2007**, *51*, 1–74.
(26) Bordiga, S.; Regli, L.; Bonino, F.; Groppo, E.; Lamberti, C.; Xiao, B.; Wheatley, P. S.; Morris, R. E.; Zecchina, A. *Phys. Chem. Chem. Phys.* **2007**, *9*, 2676–2685.
(27) Spoto, G.; Bordiga, S.; Zecchina, A.; Cocina, D.; Gribov, E. N.; Regli, L.; Groppo, E.; Lamberti, C. *Catal. Today* **2006**, *113*, 65–80.
(28) Bonino, F.; Damin, A.; Bordiga, S.; Lamberti, C.; Zecchina, A. *Langmuir* **2003**, *19*, 2155–2161.

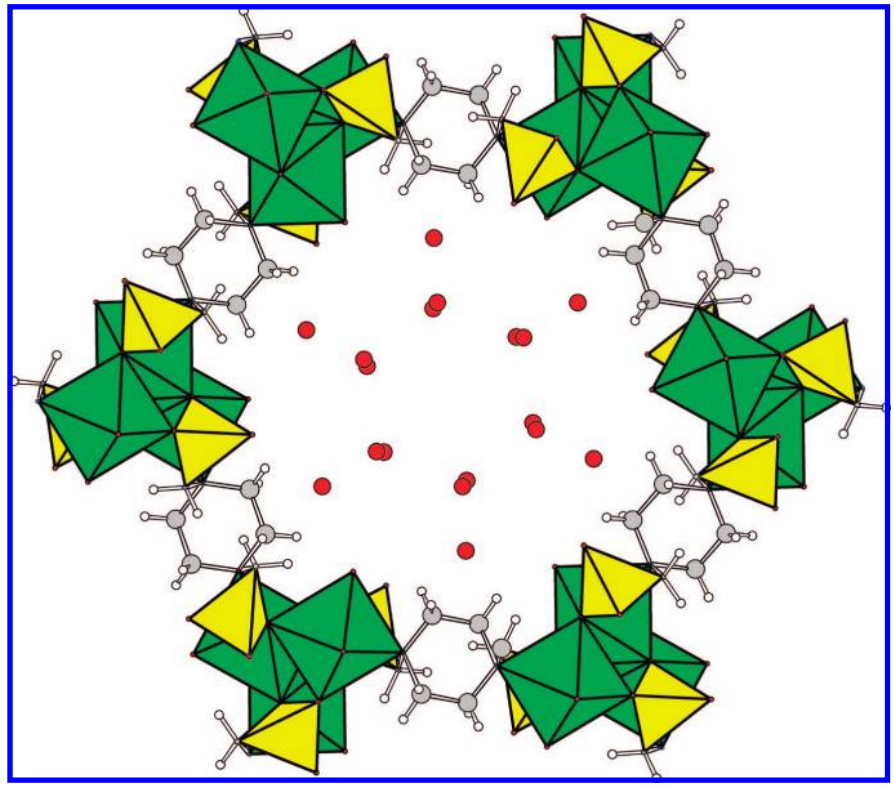

Figure 1. Framework structure of STA-12, viewed down the channel axis. All nickel octahedra in green, phosphonate tetrahedra in yellow, carbon atoms gray, and hydrogen atoms white. Oxygen atoms of physisorbed water molecules are in red.

changes occur in the first coordination sphere of Ni(II). The fully dehydrated solid displays remarkable structural complexity, including NiO_4N coordination polyhedra linked via either edge- or corner-sharing that result from a transformation mechanism that involves phosphonate group rotation. The transformation upon dehydration gives a range of adsorption sites that include coordinatively unsaturated nickel sites and accessible P═O groups. IR spectroscopic study of the interaction of these sites with adsorbed probe molecules complements the structural studies and confirms the presence of Lewis acid sites of moderate strength in the dehydrated adsorbent. The dehydrated adsorbent shows promising adsorption properties for the greenhouse gas CO_2 at room temperature.

2. Experimental Section

Ni-STA-12 was synthesised according to the published procedure.[21] In a typical preparation, 0.209 g of nickel acetate and 0.157 g of the *N*,*N*′-piperazinebismethylenehosphonic acid were dissolved in 15 mL of H_2O, and the solution was placed in a Teflon-lined Parr autoclave and heated in an oven for 3 days at 493 K. The resulting green solid was filtered and dried. The purity of the solid was checked by powder XRD on a STOE STADI/P diffractometer with a primary monochromator (Cu $K\alpha_1$, 1.54056 Å) operating in Debye−Scherrer geometry. Thermogravimetric analysis (TGA) on the sample was performed in air, with an initial isothermal stage at 300 K followed by a heating ramp at 5 K min^{-1} up to 1073 K. The structural effects of dehydration were measured by heating Ni-STA-12 in capillaries under a vacuum of 10^{-4} Torr for 4 h at temperatures between 323 and 523 K. In each case the capillary was sealed and the powder diffraction pattern measured in Debye−Scherrer geometry as described above. The solid turns yellow on dehydration. Four distinct phases were obtained during these studies: three were analyzed by synchrotron XRD, and the fourth was unstable in the synchrotron beam.

As no suitable single crystals were obtained for Ni-STA-12, the structures of the as-prepared phase, a partially dehydrated phase, and the fully dehydrated phase—the last two of which were prepared by heating under vacuum at 323 and 523 K—were determined using high-resolution powder XRD data collected on station ID-31 at the European Synchrotron Radiation Facility.[29] In all cases, data collection was carried out at 100 K in Debye−Scherrer geometry, with the sample in a 0.7 mm diameter sealed quartz capillary, with 2θ of 0−46° and using monochromated radiation with a wavelength of 0.800178(6) Å. The material was observed to change gradually in the intense beam, so 14 data collections over 2 min were performed on freshly exposed portions of each sample, with the data sets being summed. During the short data collection time (2 min), no changes occurred.

Extraction of peak positions for indexing was performed for the as-prepared and partially dehydrated samples using the EXPO2004 suite.[30] Pattern indexing was carried out within EXPO2004 using the computer program TREOR, with an absolute error on peak positions of 0.01° 2θ. For the fully dehydrated sample, it was possible to index the cell using the TOPAS suite of programs[31,32] as triclinic, $a = 6.0202$ Å, $b = 14.8731$ Å, $c = 16.1206$ Å, $\alpha = 112.5410°$, $\beta = 84.2520°$, $\gamma = 83.5250°$, $V = 1308.4$ Å^3, GOF = 145. Refined parameters obtained after a structureless whole-pattern refinement with TOPAS were $a = 6.0224(2)$ Å, $b = 14.8878(5)$ Å, $c = 16.1249(6)$ Å, $\alpha = 112.580(1)°$, $\beta = 84.303(3)°$, $\gamma = 83.504(3)°$, $V = 1310.22(8)$ Å^3. During the structure refinement, this was converted to a reduced triclinic cell ($\alpha, \beta, \gamma > 90°$).

Structures were solved *ab initio* using the EXPO2004 suite. For the hydrated materials, rhombohedral space groups of low symmetry

(29) Fitch, A. N. *J. Res. Natl. Inst. Stand. Technol.* **2004**, *109*, 133–142.
(30) Altomare, A.; Caliandro, R.; Camalli, M.; Cuocci, C.; Giacovovazzo, C.; Grazia, A.; Moliterni, G.; Rizzi, R. *J. Appl. Crystallogr.* **2004**, *37*, 1025–1028.
(31) *TOPAS V3.0*, General Profile and Structure Analysis Software for Powder Diffraction Data; Bruker AXS Ltd.: Coventry, UK, 2004.
(32) Coelho, A. A. *J. Appl. Crystallogr.* **2003**, *36*, 86–95.

Table 1. Crystallographic Data for Ni-STA-12, As-Prepared and Dehydrated under Vacuum at Different Temperatures

		dehydrated		
	as-prepared	at 323 K	at 373 K	at 523 K
formula[a]	$Ni_2L \cdot 8H_2O$	$Ni_2L \cdot 2H_2O$	$Ni_2L \cdot 0.667H_2O$	Ni_2L
unit cell composition	$Ni_{18}P_{18}O_{126}N_{18}C_{54}H_{216}$	$Ni_{18}P_{18}O_{72}N_{18}C_{54}H_{108}$	$Ni_6P_6O_{20}N_6C_{18}H_{40}$	$Ni_6P_6O_{18}N_6C_{18}H_{36}$
formula weight of unit cell	4748.3	3775.5	1198.5	1162.5
calcd density/g cm^{-3}	1.832	1.506	1.432	1.473
space group	$R\bar{3}$	$R\bar{3}$	$P\bar{1}$	$P\bar{1}$
a/Å	27.8342(1)	27.9144(1)	6.1288(7)	6.03475(5)
b/Å			15.3497(19)	14.9156(2)
c/Å	6.2421(3)	6.1655(2)	16.6292(21)	16.1572(2)
α/°			114.608(7)	112.5721(7)
β/°			98.449(14)	95.7025(11)
γ/°			94.740(32)	96.4950(11)
V/Å^3	4188.12(2)	4160.58(2)	1388.8(2)	1318.06(3)
diffractometer	ESRF/ID-31	ESRF/ID-31	Lab./STOE Stadi/p	ESRF/ID-31
temp/K	100	100	293	100
wavelength/Å	0.800178(6)	0.800178(6)	1.54051	0.800178(6)
no. reflections	521	416	not applicable	1475
no. atoms (non-H)	13	10		27
no. constraints	0	0		12
R_p	0.0411	0.0547		0.0512
R_{wp}	0.0596	0.0782		0.0694
Ls shift/su max	0.04	0.04		0.04

[a] L represents the *N*,*N*′-piperazinebismethylenephosphonate ligand.

consistent with the observed peaks were chosen as starting points and the best structural solutions taken forward for refinement. The Ni, P, O, N, and C atoms were found from the E-maps with the highest figure of merit. The corresponding atomic coordinates for each structure were used as starting models for Rietveld refinement, using the GSAS program suite,[33] and using data over the range 2−35° 2*θ*, above which the peaks became broad. A pseudo-Voigtian function was selected to describe individual line profiles. Unit cell and instrumental parameters were allowed to vary during the refinement process, as were the atomic coordinates. No restraints were applied for the hydrated or partially hydrated samples, and only P−O and P−C bond lengths for the phosphonate groups were restrained (to 1.53(1) and 1.87(3) Å, respectively) for the dehydrated sample. Removing these restraints gave a stable refinement, but with some bond distances 0.1 Å outside chemically reasonable values. Table 1 lists the crystallographic information for each structure solution. Rietveld refinements of the partially and fully dehydrated Ni-STA-12 against synchrotron data are shown in Figures 2 and 3, indicating the change in symmetry upon removal of water molecules coordinated to the nickel cations. A Rietveld plot of the refinement of the as-prepared Ni-STA-12 against synchrotron X-ray data, from which accurate locations of the physically bound water molecules have been obtained, is given in the Supporting Information. For structures of the hydrated, partially dehydrated, and fully dehydrated phases, CIF files have been deposited and the atomic coordinates, including those of hydrogen atoms placed geometrically, are also given in the Supporting Information. An additional partially dehydrated phase was also observed from laboratory XRD, following dehydration at 393 K, and this was indexed using the DICVOL program,[34] giving a triclinic cell closely related to that of the fully dehydrated material.

A nitrogen adsorption isotherm at 77 K was measured on the dehydrated form of Ni-STA-12, and direct calorimetric measurements were obtained simultaneously during the adsorption process.[35] The low-temperature calorimeter used at 77 K consists of two thermopiles of around 800 thermocouples each, mounted in electrical opposition. This system is immersed in a liquid nitrogen cryostat. Around 50 mg of sample is placed in a sample cell, which, after outgassing, is attached to a simple manometric device coupled to the calorimeter. A continuous procedure of nitrogen introduction is employed which is slow enough (approximately 2 $cm^3\ h^{-1}$) to be close to equilibrium. This procedure on the low-temperature calorimeter leads to a high resolution in both the isotherm and differential enthalpies of adsorption. Further to nitrogen adsorption, the surface was characterized by measurement on the low-temperature calorimeter of the adsorption isotherms and differential enthalpies of adsorption of carbon monoxide and hydrogen at 77 K. To confirm that the pores of dehydrated Ni-STA-12 were large enough to adsorb aromatic hydrocarbons, the vapors of toluene, *o*-xylene, and mesitylene (Acros Organics, 99+%) were allowed to contact Ni-STA-12 dehydrated at 523 K on a glass line with greaseless taps, and the weight percent uptake at 300 K was calculated from the observed pressure changes on the line. A maximum uptake was measured at a vapor pressure below the saturated vapor pressure ($p/p_o \approx 0.9$). The organics were first degassed by freeze/thaw cycles.

In order to make an initial evaluation of the adsorption properties of the Ni-STA-12 for potential storage and separation applications, adsorption of carbon dioxide and methane was carried out at 303 K. These greenhouse gases have been chosen both with respect to their relevance in several applications and also to permit a comparison between interactions of the adsorbent with molecules possessing a significant quadrupole moment (CO_2) and without any permanent moment (CH_4). Again it is possible to couple the isotherm measurement with calorimetry to gain energetic information. The "room-temperature" experiments were carried out at 303 K using a volumetric device coupled with a Tian−Calvet-type calorimeter (with over 1000 thermocouples in each thermopile), placed in a thermostat regulated to within 0.01 K. In this case, a discontinuous gas dosing procedure was used up to a pressure of 15 bar so that more widely spaced measurements of differential enthalpies are made in this apparatus. For the initial CO_2 measurements, the sample was outgassed for 72 h at room temperature in order to partially dehydrate the Ni-STA-12. Further experiments with CO_2 and CH_4 were then carried out on totally dehydrated samples outgassed at 523 K for 4 h at a residual pressure below 5×10^{-3} mbar. The various gases used for these adsorption experiments were obtained from Air Liquide and are of 99.9999% minimum purity (N60). In order to assess the selectivity of Ni-STA-12 for carbon dioxide over methane at low coverages, adsorption isotherms and differential enthalpies of adsorption at

(33) Larson, A. C.; von Dreele, R. B. *Generalized Crystal Structure Analysis System*; Los Alamos National Laboratory: Los Alamos, NM, 1998.
(34) Boultif, A.; Louer, D. *J. Appl. Crystallogr.* **2004**, *37*, 724–731.
(35) Llewellyn, P. L.; Maurin, G. *C. R. Chim.* **2005**, *8*, 283.

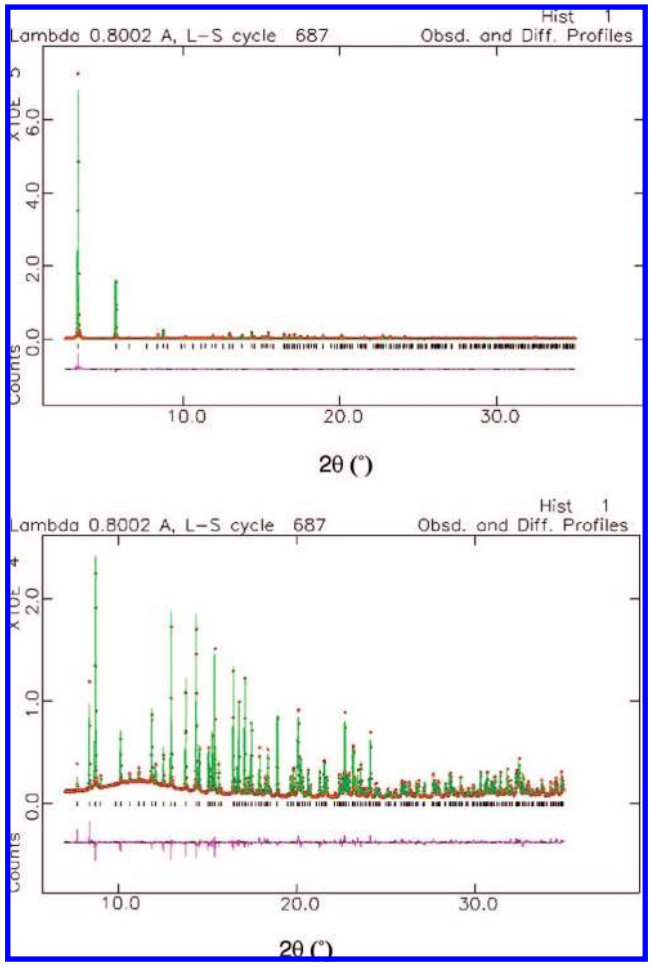

Figure 2. Rietveld plots (top, 2.5−35° 2θ; bottom, with 7−35° 2θ expanded) of synchrotron powder X-ray diffraction of partially dehydrated Ni-STA-12, from which physisorbed water molecules have been removed but which has retained the rhombohedral symmetry of the as-prepared material. The plots show experimental data and calculated and difference profiles.

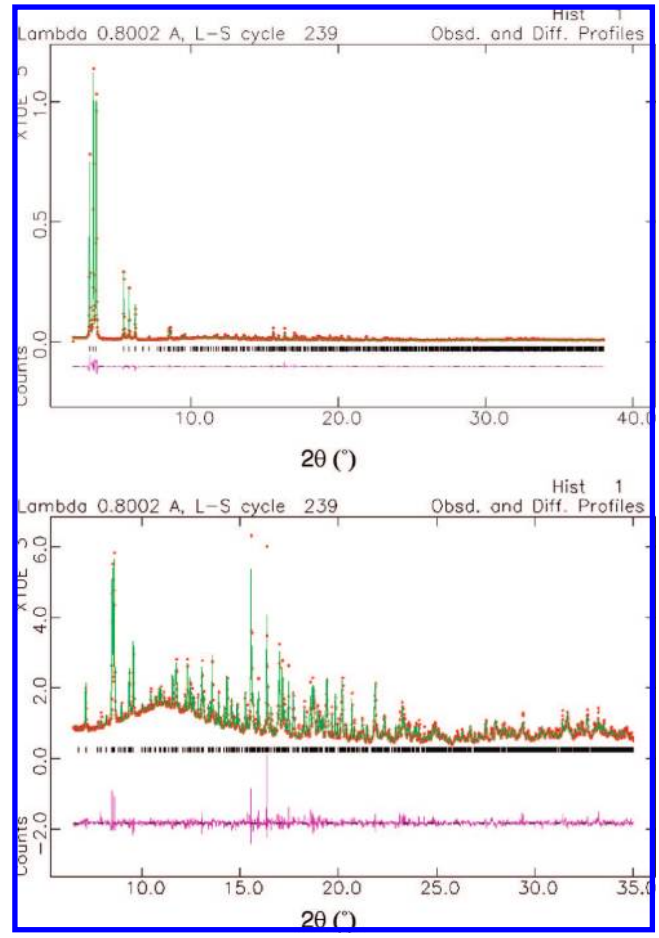

Figure 3. Rietveld plots (top, 2.5−35° 2θ; bottom, with 7−35° 2θ expanded) of fully dehydrated Ni-STA-12, which has changed symmetry to triclinic. The plot shows experimental data and calculated and difference profiles.

303 K for both carbon dioxide and methane on fully dehydrated Ni-STA-12 were also measured at higher resolution up to 1 bar.

All the infrared spectroscopic measurements were performed under controlled atmospheres by using environmental cells that allow thermal treatment under high vacuum, dosing of gases (H_2, CO, CO_2) and vapors (H_2O, CH_3OH, CH_3CN), and *in situ* spectra collection. FTIR spectra were collected in transmission mode on self-supporting wafers or on a thin film on a silicon wafer, in a controlled atmosphere, after thermal pretreatment in high vacuum at 523 K. Spectra were recorded at 2 cm^{-1} resolution on a Bruker IFS 66 FTIR spectrometer. In the case of H_2 adsorption, a Bruker Equinox-55 FTIR spectrometer was adopted, equipped with a MCT detector whose sample compartment was modified *ad hoc* to accommodate the cryogenic IR cell. A detailed description of the cryogenic cell (consisting of a modified closed-circuit liquid helium Oxford CCC 1204 cryostat) is given elsewhere.[36]

Raman spectra were recorded by using a Renishaw Raman Microscope spectrometer. An Ar^+ laser emitting at 514 nm was used, in which the output power was limited to 10% (100% power = 8.2 mW at the sample) in order to avoid sample damage. The photons scattered by the sample were dispersed by a monochromator with a 1800 lines/mm grating and simultaneously collected on a CCD camera; the collection optic was set at 20× objective. The spectra were obtained by collecting 10 acquisitions (each of 10 s) on a self-supporting wafer put in a home-made cell with a suprasil quartz cuvette that allowed measurements in controlled atmosphere. In this case the sample was measured after a thermal pretreatment in high vacuum at 523 K. Diffuse relectance−UV−vis−near-IR measurements were performed on a powdered sample in a quartz cell after thermal pretreatment in high vacuum at 523 K by using a Varian Cary 5 spectrophotometer equipped with a reflectance sphere.

3. Results and Discussion

3.1. Dehydration Behavior of STA-12. Thermogravimetric analysis of Ni-STA-12 at 5 K /min in air (Figure 4) shows water loss in at least three steps, with 18 wt % lost below 343 K and 7 wt % lost between 373 and 423 K in two steps, in the approximate ratio 2:1. The curve shows a plateau in the 423−673 K range before a progressive weight loss due to structural decomposition. Laboratory powder diffraction (Figure 5) shows that the rhombohedral symmetry of the as-prepared material is retained by evacuating at 323 K but is lost upon dehydration at 373 K, when an intermediate, further dehydrated triclinic structure has appeared. Dehydrating above this temperature gives the fully dehydrated material, which is also triclinic. The synchrotron XRD pattern of the fully dehydrated Ni-STA-12 measured at 100 K is similar to that observed in the laboratory at room temperature, indicating that the structure

(36) Spoto, G.; Gribov, E. N.; Ricchiardi, G.; Damin, A.; Scarano, D.; Bordiga, S.; Lamberti, C.; Zecchina, A. *Prog. Surf. Sci.* **2004**, *76*, 71–146.

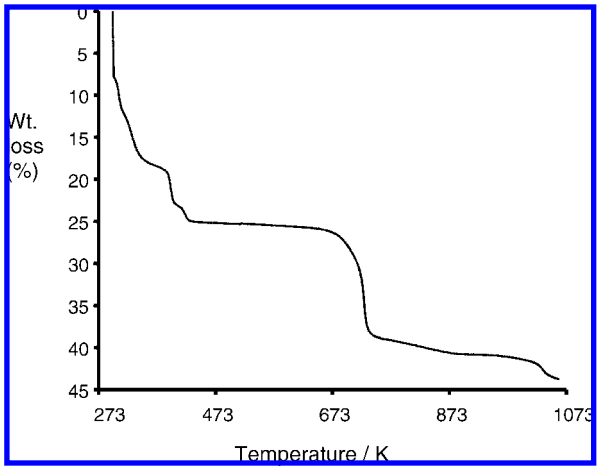

Figure 4. Thermogravimetric analysis of Ni-STA-12 measured at 5 K/min in air. The TGA clearly shows that the loss of chemisorbed water between 373 and 423 K occurs in two events.

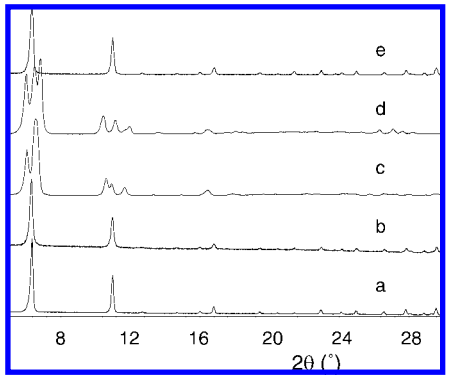

Figure 5. Laboratory X-ray powder diffraction patterns of (a) as-prepared STA-12, (b) Ni-STA-12 dehydrated at 323 K, (c) Ni-STA-12 dehydrated at 373 K, (d) fully dehydrated Ni-STA-12, and (e) rehydrated Ni-STA-12.

derived from the synchrotron data is closely similar to that on which CO_2 adsorption has been performed.

From the reported structural determination of the as-prepared Ni-STA-12 from laboratory data, the first water loss event can be associated with the removal of physisorbed water while the second and third water losses can be attributed to loss of water bound to the nickel cations, according to eq 1.

$$Ni_6(H_2O)_6L_3 \cdot 18H_2O \rightarrow Ni_6(H_2O)_6L_3 \rightarrow Ni_6(H_2O)_2L_3 \rightarrow Ni_6L_3 \quad (1)$$

On the basis of this behavior, dehydration under vacuum was performed at 323 K to remove the physisorbed water and at 523 K to give the fully dehydrated form for synchrotron diffraction experiments. Careful variation of the dehydration temperature from 363 to 393 K enabled the intermediate phase to be isolated, but it was not stable in the synchrotron beam. The laboratory XRD patterns of all four phases are shown in Figure 5. (By contrast, the dehydrated version of Ni-STA-12 prepared with *N*,*N*′-2-methylpiperazinebismethylenephosphonic acid remains rhombohedral upon dehydration.)

3.2. X-ray Diffraction, Optical, and Vibrational Spectroscopic Study of As-Prepared and Dehydrated Samples. High-resolution synchrotron X-ray powder data were collected on the as-prepared solid and also on samples dehydrated at 323 and 523 K. The additional resolution available at station ID-31 was very helpful for structure solution of the fully dehydrated sample because its symmetry is triclinic, and so the dehydrated structure is crystallographically more complex than in the rhombohedral as-prepared material. The adsorption behavior of STA-12 can only be understood in terms of the dehydrated samples.

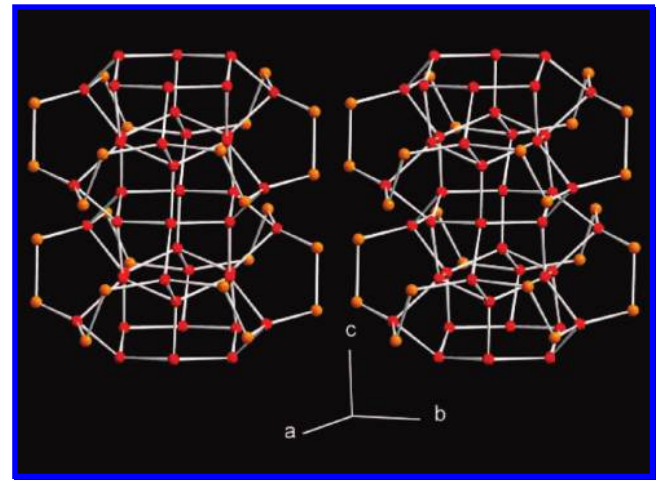

Figure 6. Stereoview showing the H-bonded array of water molecules within the pores of hydrated STA-12, as measured at 100 K. Red spheres represent oxygen atoms of physisorbed water molecules in the channels; orange spheres represent oxygen atoms bound to phosphorus and nickel atoms of the framework.

Structure solution of the hydrated and partially dehydrated forms of Ni-STA-12 (the latter evacuated at 323 K) confirms the framework structure determined from laboratory data,[21] in which the ligand is coordinated to nickel cations via two oxygen atoms and a nitrogen from the piperazine ring, leaving one phosphonate oxygen atom projecting into the pore. An oxygen atom from chemisorbed water is, in each case, coordinated to make up regular NiO_5N octahedra, which share edges to give a spiral chain along the *c* axis. The two framework structures are essentially identical, the main structural difference coming from the presence or absence of physisorbed water molecules in the pores.

For the hydrated sample, the higher resolution of the data and the low data collection temperature enable the water molecules to be located more accurately than was possible from the room-temperature laboratory X-ray data. The result is the determination of a hydrogen-bonded array of water molecules that are in turn hydrogen-bonded to phosphonate oxygen atoms projecting into the pores and the oxygen atoms of coordinated water molecules (or hydroxyl ions) on the nickel cations (Figures 1 and 6). All of the oxygen atoms of the physisorbed water molecules are tetrahedrally bound to other oxygen atoms involved in the H-bonding scheme. The water molecules adopt an array that is similar to that of hexagonal ice,[37] where layers of tetrahedrally coordinated oxygen atoms are hydrogen-bonded to similar layers above and below. Whereas in hexagonal ice all hydrogen bonds are directly between adjacent layers, in this structure one in two links between the layers of water oxygen atoms occurs through two hydrogen bonds, via an intermediate oxygen atom of a physisorbed water molecule. This columnar array is commensurate with the framework, with which it is able to make hydrogen bonds.

The fully dehydrated structure of Ni-STA-12 is, like the as-prepared solid, based on spiral chains of nickel-centred poly-

(37) Janiak, C.; Scharmann, T. G. *J. Am. Chem. Soc.* **2002**, *124*, 14010–14011.

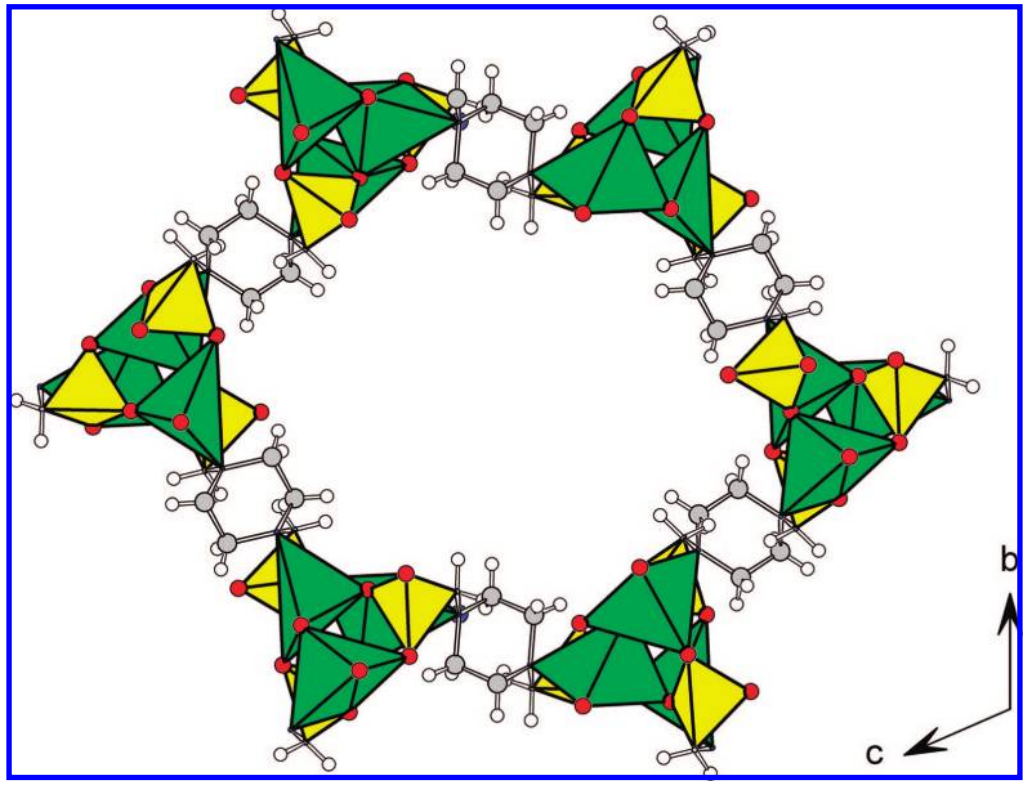

Figure 7. Structure of the dehydrated Ni-STA-12, viewed down the channel axis. Color scheme as in Figure 1.

hedra linked by bisphosphonate ligands, where the methylenephosphonate groups attached to the nitrogens are in axial positions on the piperazine rings, which adopt chair configurations (Figure 7). The structure retains large pores, as viewed down the *c* axis, although these channels are now elliptical rather than circular in cross section, with free dimensions of 8 Å × 9 Å rather than *ca*. 10 Å. The measured maximum uptakes at 300 K of dehydrated Ni-STA-12 for toluene, *o*-xylene, and mesitylene (with relevant molecular dimensions of 6 − 8 Å) were 8.9, 6.2, and 5.8 wt %, respectively, indicating that the pores of the dehydrated solids are large enough to absorb these molecules, consistent with the structure.

The loss of coordinated oxygen atoms derived from chemisorbed water molecules results in three crystallographically nonequivalent nickel cation positions instead of one, and while all the nickel cations remain coordinated to one ligand nitrogen atom, they are only coordinated by four oxygen atoms, all of which are from phosphonate groups, rather than five oxygen atoms, four from phosphonate and one from water. The structure of the spiral inorganic chains is shown in Figure 8, with NiO_4N polyhedra in the chains exhibiting both corner-sharing and edge-sharing. Ni(1)O_4N and Ni(2)O_4N share an edge, whereas Ni(1)O_4N and Ni(3)O_4N share a corner: all PO_3C tetrahedra remain corner-sharing. Two out of the three different phosphonate groups change their coordination, so that all three of their oxygen atoms as well as the piperazine nitrogen atom are bound to nickel cations. The third phosphonate group, P(3)O_3C, remains in its original configuration, with a single P═O bond projecting into the pore space, accessible to adsorbates. The change in local symmetry of Ni(II) sites that occurs upon dehydration is readily observed by UV−visible spectroscopy (Figure 9a). As-prepared Ni-STA-12 (blue curve) is characterized by the presence of an intense component at about 250 nm, associated with the organic linker and by a complex set of bands

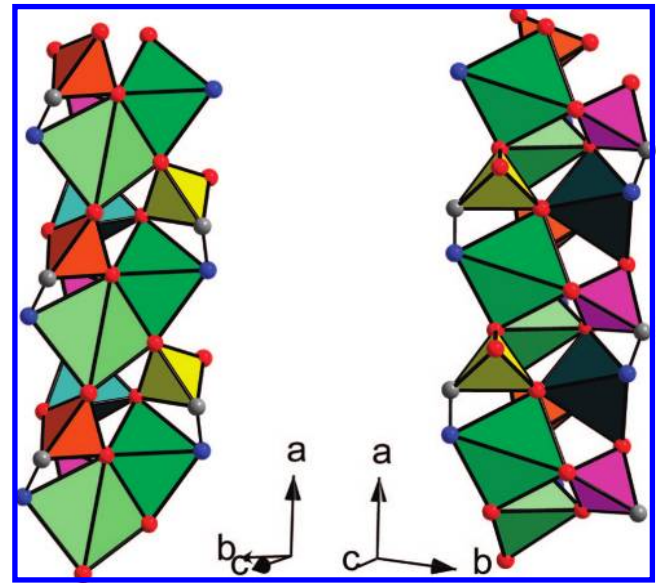

Figure 8. Two different views of the inorganic chain of dehydrated Ni-STA-12, showing crystallographically distinct NiO_4N and PO_3C polyhedra in different colors. Ni(1), light green; Ni(2) medium green; Ni(3) dark blue-green; P(1) orange; P(2) yellow; P(3) purple.

in the region of metal d−d transitions (visible and near-infrared) that comprise a contribution at 420 nm, double peaks at 695 and 770 nm, a band at 1280 nm, and a further component at 1950 nm. For Ni(II) in O_h symmetry, only three weak bands due to spin-allowed d−d transitions would be expected,[2] so the appearance of the fourth band in the near-infrared region must be explained by the presence of nitrogen inside the first coordination sphere of Ni(II) sites that disrupts their symmetry. Thermal treatment *in vacuo* at 523 K produces major changes

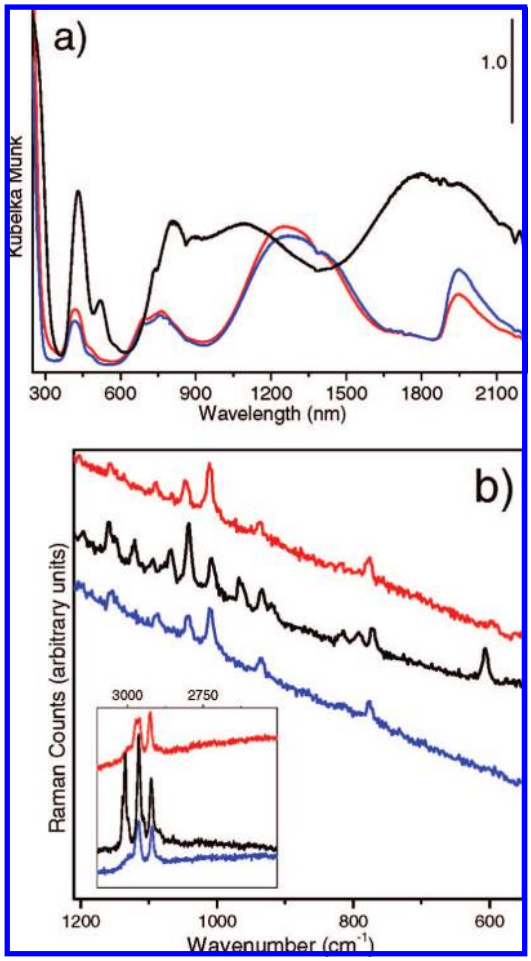

Figure 9. Reversible effect of water removal: blue curves, as-prepared; black curves, dehydrated at 523 K; red curves, rehydrated samples. (a) Diffuse reflectance UV−vis−NIR of STA-12. (b) Dispersive Micro Raman with 514 nm exciting line.

in the optical spectrum of the Ni-STA-12 (black curve), especially for the d−d bands (new maxima at 428, 518, 810, 1090, 1800, and 1955 nm), while the contribution due to the organic linker shows only a modest red shift. The number of bands and their broad character suggest that NiO_4N polyhedra are intermediate between tetragonal pyramids and trigonal bipyramids.[38] This indicates that the removal of water molecules directly coordinated to Ni(II) species causes a substantial modification of the electronic structure of the metal as a result of changes in symmetry and ligand field. These structural changes are fully reversible upon rehydration, as illustrated by the red curve reported in Figure 9a.

The structural reorganization required to transform from hydrated to dehydrated Ni-STA-12 is shown in Figure 10, where the inorganic chain of the dehydrated structure is compared with that of the as-prepared material, viewed from two different directions. Whereas each nickel and each phosphonate group is equivalent in the starting material, in the triclinic structure there are three distinct nickel sites and three distinct phosphonate groups, which are colored differently in the figures. The structural rearrangement occurs by loss of the coordinated water molecules from all nickel cations, followed by rotation of two out of three of the phosphonate groups (which become $P(1)O_3C$ and $P(3)O_3C$ in the triclinic structure) to allow their full corner-sharing with nickel cations. The third phosphonate group does not change coordination, leaving a P═O group protruding into the pore ($P(2)O_3C$ in the fully dehydrated structure).

From these structural data, it is possible to understand why STA-12 prepared with the *N*,*N*′-2-methylpiperazinebismethylenephosphonic acid does not distort from rhombohedral to triclinic upon hydration.[21] Whereas there is enough space for methyl groups in equatorial positions on the piperazine rings in the fully hydrated structure, these methyl groups would have unreasonably close distances of approach to phosphonate oxygen atoms in a hypothetical dehydrated 2-methyl material with the same triclinic distorted framework structure. Indeed, measured distances between equatorial H atoms and framework oxygen atoms in the dehydrated structure are, at 2.45 Å, only just large enough to accommodate the H and O van der Waals radii, and the methyl groups would be too large. As a result, the structure of Ni-STA-12 remains rhombohedral after dehydration, albeit with relatively low crystallinity, and because it does not distort to give narrower channels, as the non-methyl form does, the solid displays a higher pore volume than the non-methyl structure, even though methyl groups project into the channels.[21]

Although the positions of the Ni, P, O, C, and N atoms in hydrated and dehydrated STA-12 are located by the X-ray experiments, and the hydrogen atoms on the carbon atoms of the ligand can readily be placed geometrically, ambiguities remain about the location of some of the protons in the hydrated samples. This aspect has been investigated by Raman and infrared spectroscopies that have been performed on the hydrated and dehydrated samples.

Raman spectra of the as-synthetized, dehydrated, and rehydrated samples of STA-12 are reported in Figure 9b with the same color code as that used for the DR−UV−vis−NIR spectra. As-prepared and rehydrated samples show a doublet in the ν(CH) stretching region ascribed to asymmetric and symmetric modes of CH_2 units (2964 and 2915 cm^{-1} bands) that becomes a triplet in the dehydrated sample (a new band at 3008 cm^{-1}). Water removal also causes substantial changes in the low-frequency range, where the main contributions of ν(P−O) of the phosphonate groups are expected.[39−42] In this region, the hydrated samples show main bands at 1056, 1086, 1041, 1009, and 934 cm^{-1}, while the dehydrated sample is characterized by extra peaks at 1121, 1068, 960, and 600 cm^{-1} that are consistent with the change in symmetry of the phosphonates.

The IR spectrum of the completely hydrated sample (black dot-dashed curves at the tops of Figure 11a,b) in the high-frequency region (3800−1500 cm^{-1}) is dominated by strong bands due to hydrogen-bonded adsorbed water (two strong and broad bands centered at 3300 cm^{-1} and a band at 1630 cm^{-1} due to stretching ν(OH) and bending δ(OH)). Sharp bands at 2920 and 2990 cm^{-1} due to the two symmetrically distinct methylene C−H vibrations are observed on the low-frequency side of the broad band assigned as ν(OH). In the low-frequency region (Figure 11b), the spectrum obtained on the as-prepared, hydrated sample is characterized by many framework vibrations, with the following assignments: bands due to δ and γ modes

(38) Ciampolini, M. *Inorg. Chem.* **1966**, *5*, 35–40.
(39) Bauer, S.; Marrot, J.; Devic, T.; Férey, G.; Stock, N. *Inorg. Chem.* **2007**, *46*, 9998–10002.
(40) Bakhmutova, E. V.; Ouyang, X.; Medvedev, D. G.; Clearfield, A. *Inorg. Chem.* **2003**, *42*, 7046–7051.
(41) Stock, N.; Bein, T. *J. Solid State Chem.* **2002**, *167*, 330–336.
(42) Zima, V.; Svoboda, J.; Benesà, L.; Melànovà, K.; Trchová, M.; Dybal, J. *J. Solid State Chem.* **2007**, *180*, 929–939.

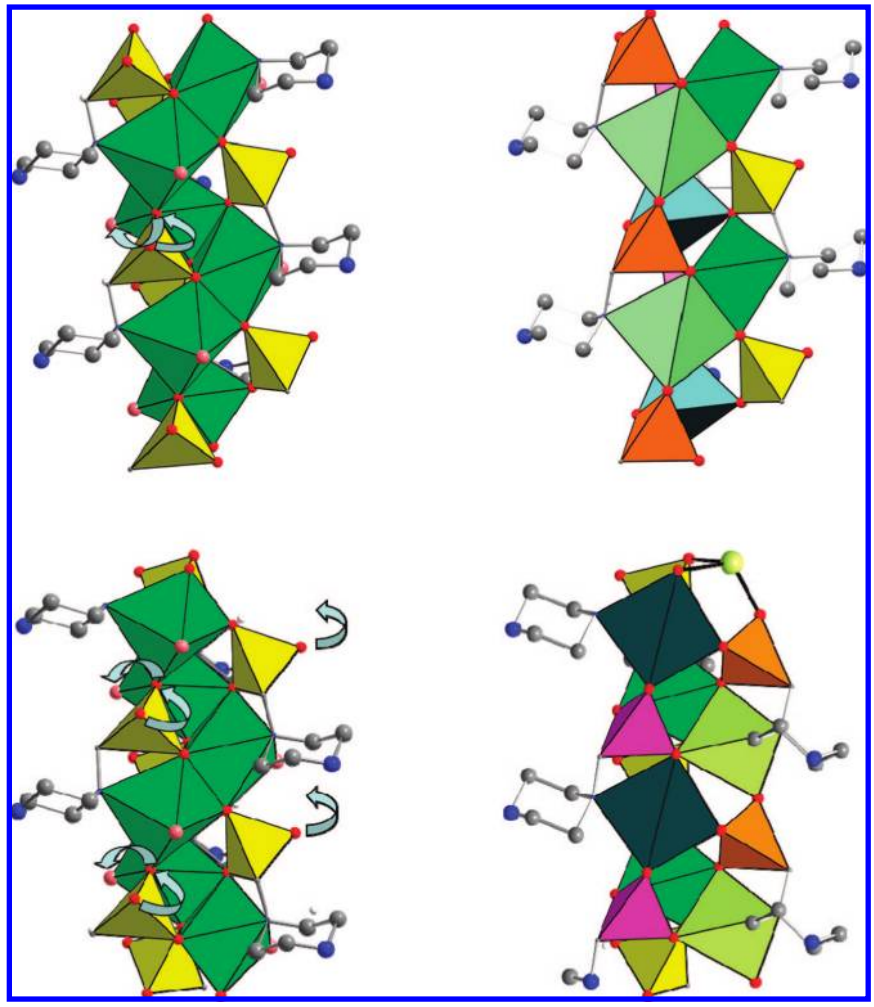

Figure 10. Two different comparisons of the inorganic chains and coordinated piperazine rings for the as-prepared and dehydrated Ni-STA-12 structures, showing by blue arrows the structural rearrangements that give rise to the structure change that occurs upon loss of water molecules coordinated to nickel cations (the oxygen atoms of which are represented as pink spheres). Color scheme for polyhedra as in Figure 8.

of CH_2 groups of the piperazine ligand (1460 and 1373 cm^{-1}); absorptions due to ν(C−C) and ν(C−N) combined with features associated with the ν(P−O) of the phosphonate groups (1160−950 cm^{-1}); symmetric and antisymmetric bending modes of CPO_3 units (triplet at 580, 530, and 508 cm^{-1}).[39−42]

Dehydration under vacuum at 523 K results in a substantial change in the infrared spectrum (shown at the bottoms of Figure 11a,b as bold black curves). As expected, all the features associated with water disappear (strong and broad bands centered at 3300 cm^{-1} and the band at 1630 cm^{-1}), while the C−H vibrational spectrum becomes more complex, with splittings resulting from the symmetry change: the dehydrated sample possesses nine distinct C atoms, the as-prepared only three. There are also important changes in the framework region, with an evident perturbation of nearly all the bands that appear better resolved, sometimes more intense, and slightly shifted with respect to the hydrated material. Moreover, the appearance of a strong band at 1207 cm^{-1} and the modification of the spectrum in the ν(P−O) and bending CPO_3 regions suggest the formation of P═O groups and the distortion of the CPO_3 units (the main component appears at 590 cm^{-1}, and a new band appears at 490 cm^{-1}).

Stepwise dosing of the sample with H_2O results in a complex spectral evolution. For clarity, the spectra are reported in Figure 11 with *y*-axis shifts in three separate blocks that correspond to three different phases of the hydration process. At low H_2O coverages (the red curves), the growth of a sharp band at 3685 cm^{-1} indicates the formation of isolated OH groups, whereas broad absorption bands centered at 2700 and 1590 cm^{-1} are attributed to the stretching and bending modes of OH groups in a strongly hydrogen -bonded system.[43,44] The C−H stretching region becomes dominated by two bands, presumably as the symmetry increases to rhombohedral. There is simultaneous erosion of the band at 1207 cm^{-1} associated with P═O groups as a result of their reaction with adsorbed water. In addition, there are changes in the ν(P−O) region, where the bands at 1126, 1072, and 959 cm^{-1} decrease while components at 1150, 1026, and 977 cm^{-1} grow. There is also erosion of the band at 590 cm^{-1} and parallel formation of a component at 568 cm^{-1} (with an isosbestic point at 582 cm^{-1}), growth of the bands at 530 and 510 cm^{-1}, and decrease of the band at 496 cm^{-1}, all of which can be explained in terms of a significant perturbation of the CPO_3 units. Finally, a broad absorption appears at 626 cm^{-1} that could be associated with the bending mode of a NiOH species. These features arise because the water does not simply coordinate to the nickel but reacts with the phosphonate, giving

(43) Zecchina, A.; Spoto, G.; Bordiga, S. *Phys. Chem. Chem. Phys.* **2005**, *7*, 1627–1642.
(44) Zecchina, A.; Geobaldo, F.; Spoto, G.; Bordiga, S.; Ricchiardi, G.; Buzzoni, R.; Petrini, G. *J. Phys. Chem.* **1996**, *100*, 16584–16599.

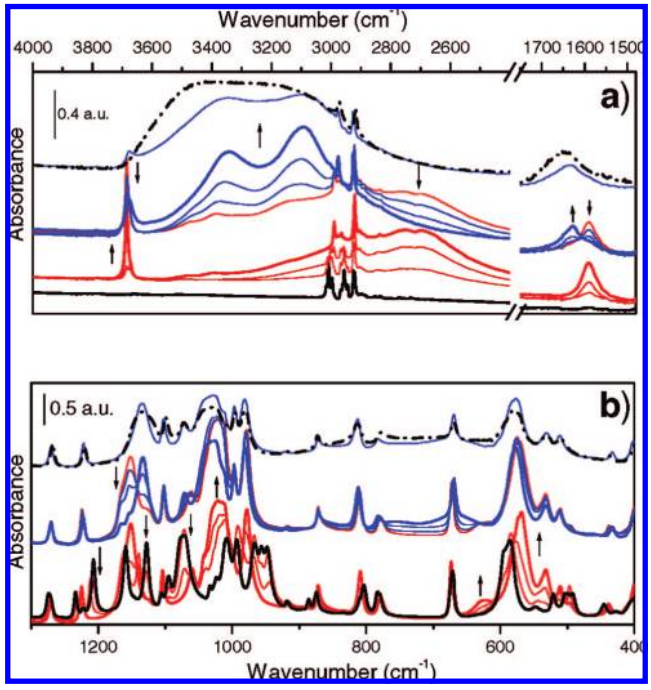

Figure 11. Effect of hydration/dehydration on IR spectra of Ni-STA-12. (a) OH stretching and bending region. (b) Framework modes region. Bold black dot-dashed curves at top, hydrated sample; black curve at bottom, dehydrated sample; red curves, low H_2O coverages; blue curves, medium to high coverages.

Scheme 1

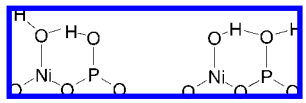

rise to NiOH and POH species, and at the same time changes the phosphonate coordination.

On the basis of this IR evidence and a knowledge of the structure of the dehydrated and partially hydrated solids, it is clear that the adsorption of water in this first stage generates two sorts of hydroxyl groups, one strongly hydrogen-bonded and the other free. Knowing the location of atoms other than hydroxyl protons from the water in the partially hydrated solid, the two possible configurations are a free NiOH group and a hydrogen-bonded POH-ONi or *vice versa*, as suggested in Scheme 1. The free OH groups do not show an acidic character, because when CO is used as a probe molecule onto them, no shift in frequency is observed. It is therefore thought that they are more likely to be NiOH groups.

An intermediate phase is identified from XRD of dehydrated Ni-STA-12, which is thought, on the basis of the stepwise dehydration observed by TGA, to have the unit cell formula $Ni_6(H_2O)_2L_3$. If dehydration is truly reversible, then the stoichiometry suggests the phase could also be formed by coordination of a water molecule to one in three nickel cations of the fully dehydrated structure. Erosion of the resonance at 1207 cm^{-1} attributed to the P═O bond is observed immediately upon hydration, so the first water molecule is expected to react with the P═O/Ni^{2+} pair to give POH and NiOH groups in the complex structure shown in Scheme 1.

Further hydration must enable the remaining fully coordinated phosphonate groups to react so that one of the P−O bonds in each CPO_3 group points into the pores, as observed experimentally. The mechanism for this involves the coordination of an incoming water molecule at a nickel cation site, which displaces the phosphonate oxygen from that nickel and results in rotation of that phosphonate group so that one phosphonate PO group ends up projecting into the pore (Figure 10).

Scheme 2

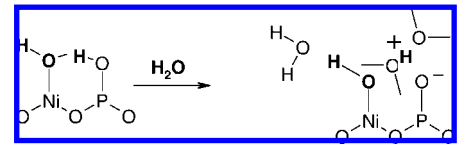

At intermediate coverages (the middle spectra of Figure 11a,b), the main changes occur in the high-frequency region as water molecules are physisorbed into the channels. The narrow band at 3680 cm^{-1} progressively decreases as these OH groups form weak H-bonds with incoming water molecules. The H-bonded OH groups represented by the band at 2700 cm^{-1} decrease in importance as the spectra become dominated by two maxima at 3100 and 3400 cm^{-1} and the band at 1590 cm^{-1} decreases, while a new component at 1630 cm^{-1} increases. The two apparent maxima at 3100 and 3400 cm^{-1} may be explained by considering the formation of an Evans window at 3200 cm^{-1} due to Fermi resonance with two δ(OH) groups of H-bonded water.[43,44] In the framework stretching region (Figure 11b), the erosion of the band at 1150 cm^{-1} with the parallel growth of a band at 1132 cm^{-1} (isosbestic point at 1140 cm^{-1}) suggests that PO_3 units undergo further changes in symmetry. Finally, the band at 626 cm^{-1} decreases, shifts to higher frequency, and broadens, in agreement with the disappearance of isolated NiOH.[41] The erosion of the band at 1590 cm^{-1} and the parallel growth of a new component at 1630 cm^{-1} (isosbestic point at 1607 cm^{-1}) suggest the evolution of the species formed in the first hydration step toward new structures where NiOH forms weak H-bonds with water and the cyclic structure reported in Scheme 1 gives rise to solvated protons, as suggested in Scheme 2. Very similar data have been obtained in the case of H_2O adsorbed in acidic zeolites.[43,44] These changes are consistent with the stepwise addition of water molecules at the inner surface of the pores, where they form a hydrogen-bonding network with OH groups attached to nickel cations and phosphorus atoms.

In the presence of a large amount of adsorbed water, as shown by the top spectra Figure 11a,b, the complete erosion of the isolated OH groups and the formation of a single, very broad absorption centered at 3300 cm^{-1} are observed. In this condition, water has filled the pores, giving a complete hydrogen-bonded network, and no more free OH groups are available. The low-temperature fully hydrated structure indicates the tendency for these water molecules to order within the pores via hydrogen-bonding. The spectrum obtained after equilibration is indistinguishable from that collected on the as-prepared material.

The reactivity of P═O species was investigated further by following the spectroscopic evolution upon interaction of the dehydrated Ni-STA-12 with CH_3OH. The results of sequential adsorption of methanol onto Ni-STA-12 are described in the Supporting Information: the experiment confirms the reactivity of both P═O and Ni sites and their different acid−base character.

3.3. Low-Temperature Adsorption and Investigation of Adsorption Sites in Ni-STA-12 by IR of the Probe Molecules H_2 and CO. Once dehydrated, STA-12 exhibits considerable pore volume for the adsorption of gases. At 77 K, the N_2

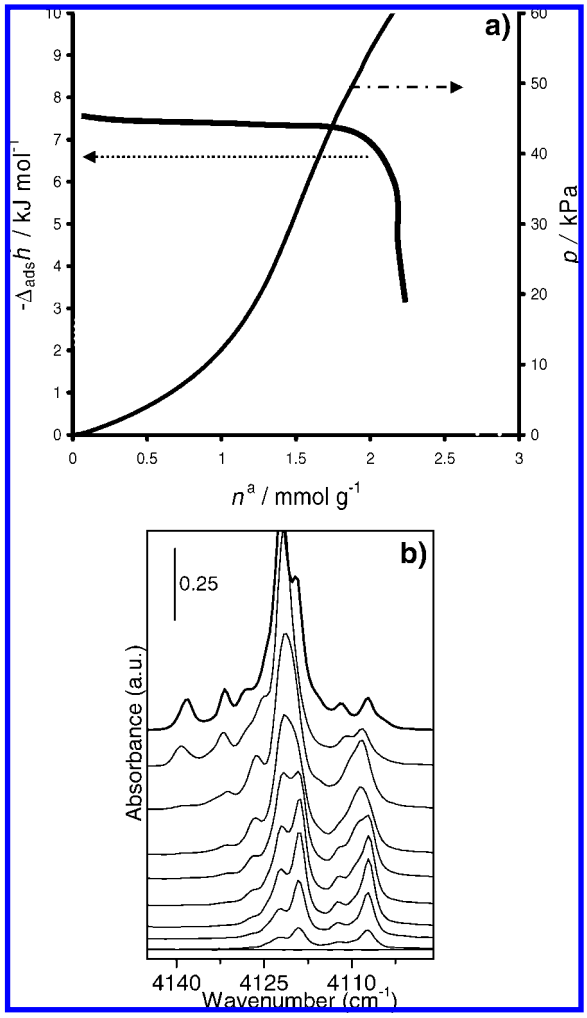

Figure 12. (a) Adsorption isotherm and differential heats of adsorption for H_2 at 77 K on fully dehydrated Ni-STA-12. (b) IR spectra at increasing coverage of hydrogen adsorbed at 20 K on Ni-STA-12. The spectra are background-subtracted and shifted on the *y* axis for clarity.

adsorption isotherm on the dehydrated solid is close to Type I, with a micropore volume of around 0.20 cm^3 g^{-1} (at p/p_o = 0.1) (see Supporting Information).

Consideration of the structure of the dehydrated forms of Ni-STA-12 suggests a range of possible adsorption sites are present, including coordinatively unsaturated nickel metal cations in three different environments, P═O groups projecting into the pores, and organic groups linking the inorganic chains. To investigate the nature of these sites, probe molecules whose IR spectra are strongly affected by the sorbate−sorbent interaction have been adsorbed and their spectra measured. H_2 and CO were chosen as suitable probe molecules because they are small enough to reduce the effects of steric interactions and the effects of interactions on their spectra are well studied.[25−28] The H_2 and CO adsorption isotherms and differential enthalpies were measured at 77 K to complement the IR data.

The adsorption of hydrogen shows a constant enthalpy of *ca.* −7.5 kJ mol^{-1} up to a loading of around 2 mmol g^{-1} (Figure 12a). This is a higher enthalpy than for many carbon-based materials but lower than those observed with other MOFs with coordinatively unsaturated metal sites, such as MIL-100 (−11 kJ mol^{-1}), MIL-101 (−9 kJ mol^{-1}),[45] or CPO-27-Ni (−13.5 kJ mol^{-1}).[46] The structural study indicates that there are 5.2 mmol of Ni^{2+} g^{-1} in the dehydrated material. This suggests that the adsorption occurs mainly on only one of the three Ni^{2+} centers, probably because the other nickel cations are poorly accessible (Figure 13) and the hydrogen does not interact strongly enough with the nickel cations to permit the structure to distort to coordinate them more effectively (as it does for water, for instance). The constant enthalpy with filling is in contrast with the behavior of many other systems, where the interactions change with increasing coverage. The constant enthalpy suggests the interaction of hydrogen with equivalent sites without any significant lateral H_2-H_2 interactions.

It should be noted, however, that the enthalpy of adsorption calculated at low hydrogen loading is only one of the important parameters required for a material that would find application in hydrogen storage.[46] Materials with a modest enthalpy of adsorption (10.1 kJ mol^{-1}) show a total H_2 uptake of 6.9 wt % at 77 K and 90 bar.[47]

The adsorption of hydrogen (H_2) at low temperature is a well-understood infrared probe of adsorption sites on surfaces, because interaction of the molecule with the surface induces a dipole into the molecule so that the H−H vibration becomes infrared active, and the shift in the vibration frequency with respect to that of the unperturbed molecule (4160 cm^{-1}) gives an indication of the strength of the adsorption interaction. The progressive desorption of hydrogen adsorbed at 20 K on the surface of STA-12 shows a complex evolution. For clarity, the background-subtracted spectra reported in Figure 12b are described from low to high coverages. The most reactive sites adsorb hydrogen, giving a doublet at 4107 and 4119 cm^{-1}. Surprisingly, these two maxima evolve in a parallel way, suggesting a very similar interaction energy. No specific evidence of hydrogen interacting with P═O is observed. Upon increasing the coverage, two extra bands on the high-frequency sides of the two main peaks grow (maxima at 4122 and 4112 cm^{-1}), then progressively the four bands give rise to two broad bands with maxima at 4121 and 4108 cm^{-1}. At this point a new band at 4126 cm^{-1} appears. Finally, the spectrum obtained at the highest hydrogen coverage (bold curve in Figure 12b) shows hydrogen reorganization inside the channels, leading to new maxima at 4139 and 4132 cm^{-1}, a new component at 4119 cm^{-1}, and a decrease in intensity of the components at low frequency (now maxima again at 4107 and 4112 cm^{-1}). Hydrogen adsorption is completely reversible at 20 K, confirming the low interaction energy. Complex spectra evolving upon hydrogen adsorption in MOFs have previously been discussed.[26,46,48] In the case of CPO-27-Ni, the adsorption gave rise to bands at 4035 and 4028 cm^{-1} for hydrogen directly interacting with open Ni(II) sites with an adsorption enthalpy of −13.5 kJ mol^{-1}.[46] The lower interaction energy and the higher observed frequency for H_2 on Ni-STA-12 are probably because phosphonate oxygen atoms partially shield the nickel cation, which has strongly distorted tetragonal prismatic coordination. These local environments vary between the three nickel sites in the triclinic dehydrated structure (each present at 1.7

(45) Latroche, M.; Surble, S.; Serre, C.; Mellot-Draznieks, C.; Llewellyn, P. L.; Lee, J.-H.; Chang, J.-S.; Jhung, S. H.; Férey, G. *Angew. Chem., Int. Ed.* **2006**, *45*, 8227–8231.
(46) Vitillo, J. G.; Regli, L.; Chavan, S.; Ricchiardi, G.; Spoto, G.; Dietzel, P. D. C.; Bordiga, S.; Zecchina, A. *J. Am. Chem. Soc.* **2008**, *130*, 8386–8396.
(47) Dinca, M.; Dailly, A.; Liu, Y.; Brown, C. M.; Neumann, D. A.; Long, J. R. *J. Am. Chem. Soc.* **2006**, *128*, 16876–16883.
(48) Bordiga, S.; Vitillo, J. G.; Ricchiardi, G.; Regli, L.; Cocina, D.; Zecchina, A.; Arstad, B.; Bjørgen, M.; Hafizovic, J.; Lillerud, K. P. *J. Phys. Chem. B* **2005**, *109*, 18237–18242.

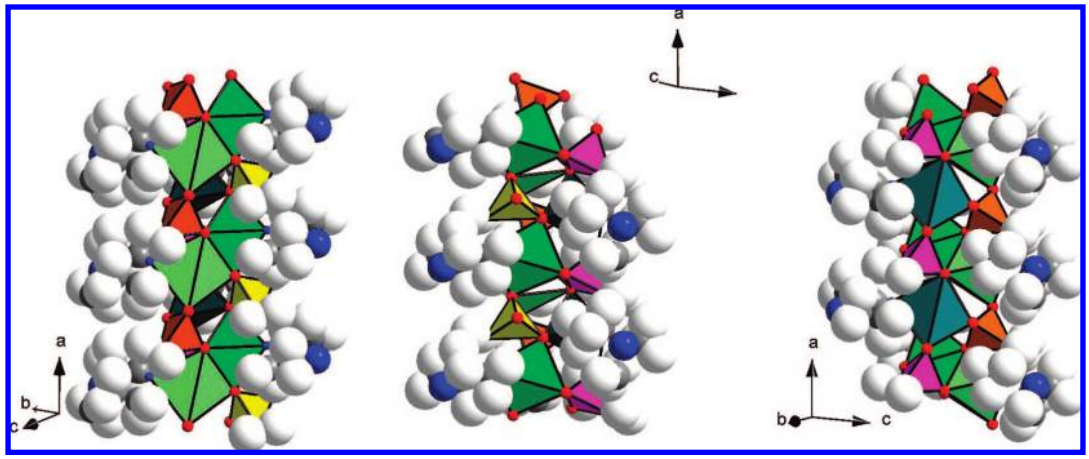

Figure 13. Structural diagrams (space-filling for H atoms) showing the different accessibility of the three distinct Ni^{2+} sites in dehydrated Ni-STA-12. Color scheme for polyhedra as in Figure 8.

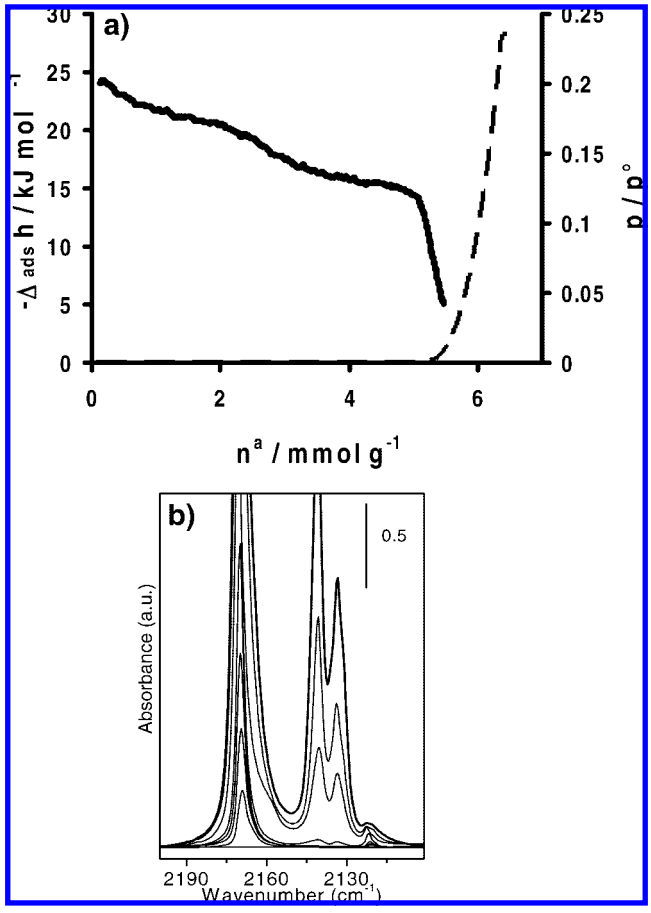

Figure 14. (a) Adsorption isotherm (dashed line) and differential heat of adsorption (solid line) for CO at 77 K on fully dehydrated Ni-STA-12. (b) Background-subtracted IR spectra of increasing coverages of CO at 77 K on Ni-STA-12.

mmol g^{-1}, Figure 8). Access to the three different Ni sites is impeded differently by the ligands, and access to Ni(2) is also impeded by the P═O oxygen atom (Figure 14). Ni(3) is the most accessible of the three metal sites, and uptake on this site could account for most of the low-pressure uptake of H_2 on Ni-STA-12 at 77 K.

Studies of the adsorption of CO on Ni-STA-12 at 77 K showed that uptakes of *ca.* 6 mmol g^{-1} were achieved, with the differential enthalpies of adsorption decreasing from 24 kJ mol^{-1} initially to 14 kJ mol^{-1} at 5 mmol g^{-1}. There appear broadly to be two adsorption regimes, with enthalpies in the ranges 19−24 kJ mol^{-1} (0 − 2 mmol g^{-1}) and 14−17 kJ mol^{-1} (2 − 5 mmol g^{-1}), confirming energetic heterogeneity of adsorption (Figure 14a). The two-step adsorption behavior is similar to that observed during the adsorption of simple gases on carbon nanotubes,[49] which was interpreted as the adsorption on two types of relatively homogeneous adsorption sites. The two adsorption regimes can be related to adsorption on all of the nickel cations. The first, higher energy adsorption step occurs up to around 2 mmol g^{-1}, similar to the total amount of hydrogen molecules adsorbed on this sample. It may be that the same sites are responsible for the H_2 adsorption and the high-enthalpy CO adsorption regime. The second, lower energy adsorption regime for CO would then correspond to completion of the CO adsorption on the other, less favorable or less accessible Ni centers. The stronger interaction with CO may indicate that the structure is able to relax to allow access of CO to more than one kind of nickel site.

Interestingly, the yellow dehydrated sample changes color to green after carbon monoxide adsorption (the same green color as that of the hydrated sample). No such color changes are observed during the adsorption of hydrogen or nitrogen. It would thus seem that the carbon monoxide is able to change the electronic configuration of the solid via a strong adsorption at nickel sites. This color change is associated with irreversible adsorption at 77 K. However, when the sample was warmed to room temperature under high vacuum, the reverse color change occurred, with a complete desorption of the adsorbed carbon monoxide.

The effects on the IR spectra of increasing coverages of CO are reported, after background subtraction, in Figure 14b. Starting from the low coverages, the growth of a band at 2170 cm^{-1} with a tail at 2164 cm^{-1} is observed. At the same time, a weak, complex band is observed at 2122 cm^{-1}. In cation-exchanged zeolites, CO adsorbs on the Lewis acidic extraframework cations via interaction of the anti-bonding HOMO of CO, which is similar to a lone pair on carbon, and high-frequency bands associated with ^{12}CO linearly bonded through the carbon to uncoordinated Ni(II) sites are observed: a similar interaction

(49) Muris, M.; Dufau, N.; Bienfait, M.; Dupont-Pavlovsky, N.; Grillet, Y.; Palmari, J. P. *Langmuir* **2000**, *16*, 7019–7022.

is observed here, but with a lower frequency shift. (The weak counterpart observed at lower frequency may be due to the analogous ^{13}CO species,[50] again with a smaller shift than expected for adsorption at a bare Ni^{2+} cation.) These lower observed shifts are attributed to the steric effects of ligands around the nickel in the NiO_4N polyhedra. At higher loading, together with "liquid-like" CO condensed inside the channels (which gives rise to the band centered at 2140 cm^{-1}), a further component at 2133 cm^{-1} is observed. This band can be associated with carbon monoxide slightly perturbed by P═O sites.[26,27] The red shift is attributed to the fact that, in this case, the interaction occurs by electron donation from the oxygen of the P═O sites to the 2π antibonding orbital of CO. This interaction is very weak and is only observed at low temperature. Conversely, the main band at 2170 cm^{-1} is associated with a stable adduct that is only partially reversible at 77 K. In order to remove all the adsorbed CO, a progressive temperature increase is required.

3.4. Performance of Ni-STA-12 as an Adsorbent at Room Temperature. Dehydrated Ni-STA-12 shows permanent porosity. In order to examine the performance in a potentially important room-temperature application, the adsorption of carbon dioxide and methane was measured up to 15 bar at 304 K, conditions of relevance for pressure swing adsorption applications. Deuterioacetonitrile (CD_3CN) was used as an IR probe molecule to investigate adsorption sites in the dehydrated sample at room temperature. CD_3CN is a widely used probe for Brönsted and Lewis acid sites. These experiments indicated that the sites present at room temperature (at which the carbon dioxide and methane adsorption experiments were carried out) are very similar to those observed by low-temperature IR measurements of adsorbed CO. Full results are given in the Supporting Information.

Isotherms and associated differential enthalpies of adsorption of carbon dioxide were measured on a sample after dehydration for 72 h at room temperature, when the physisorbed water is removed, leaving only chemisorbed water (as shown by IR spectroscopy), and also after dehydration under vacuum at 523 K, under which conditions the sample would be fully dehydrated. For methane, the adsorption isotherm and enthalpies of adsorption were measured on the fully dehydrated sample. The results are compared in Figure 15, panels a and b. Adsorption isotherms and associated differential enthalpies of adsorption were also measured at higher resolution for CO_2 and CH_4 at 0−1 bar at 303 K (Figure 16).

Uptake of carbon dioxide on the fully dehydrated solid achieves 6 mmol g^{-1} at 15 bar, with enthalpies of adsorption of 30−35 kJ mol^{-1} for most of the initial range of adsorption values, reaching a maximum at 4 mmol g^{-1} and then decreasing. This loading of 6 mmol g^{-1} corresponds approximately to the adsorption of one CO_2 molecule per nickel center in the STA-12 structure. The enthalpies of adsorption increase as the uptake increases from 0.5 to 4 mmol g^{-1}, which could be the result of the adsorption on an energetically "homogeneous" pore structure with constant energy, where the increase is due to increasing CO_2−CO_2 interactions. The decrease in enthalpies would then be due to the final stages of adsorption, where a rearrangement of the first adsorbed molecules is required to completely fill the pores.

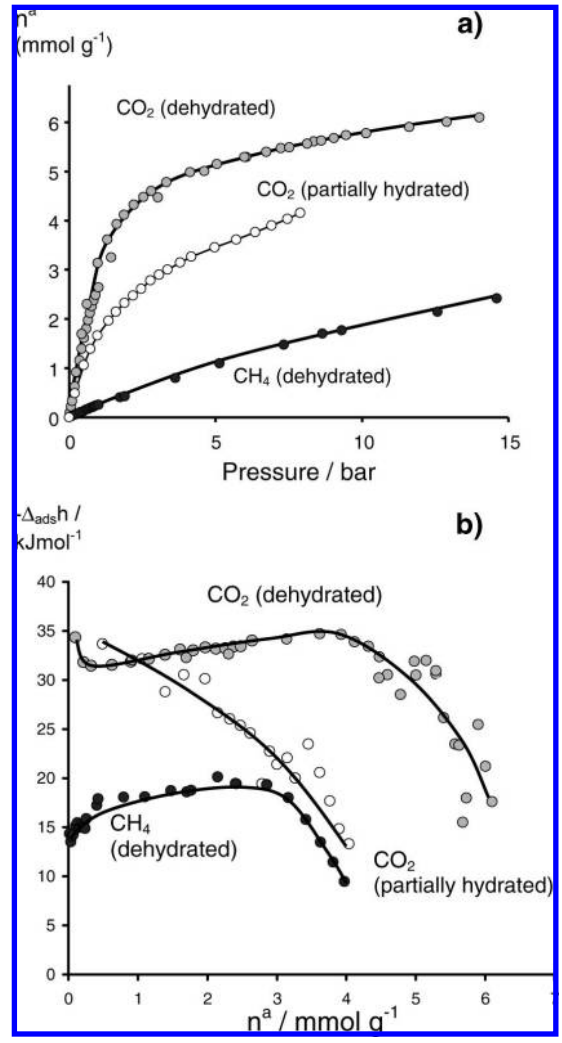

Figure 15. (a) High-pressure adsorption isotherms and (b) differential heats of adsorption measured for CO_2 at 304 K on Ni-STA-12 in partially dehydrated (white symbols) and fully dehydrated (gray symbols) forms, compared to CH_4 uptake at 304 K on fully dehydrated Ni-STA-12 (black symbols).

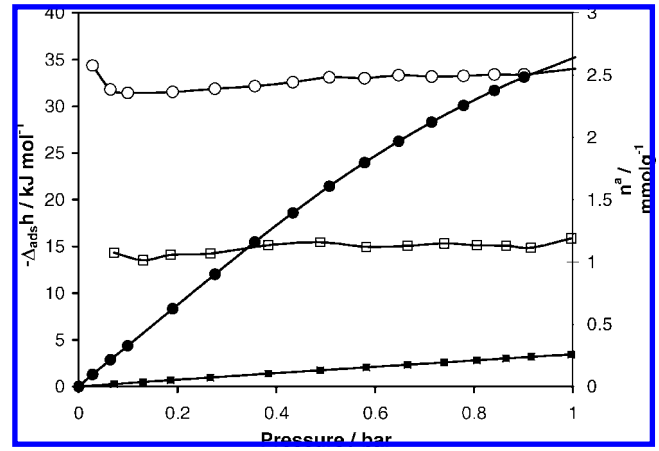

Figure 16. Adsorption isotherms from 0 to 1 bar (solid symbols) and differential heats of adsorption (open symbols) measured for CO_2 (circles) and CH_4 (squares) at 304 K on Ni-STA-12 in the fully dehydrated form.

The enthalpies of adsorption in the range of 30−35 kJ mol^{-1} for CO_2 on the dehydrated Ni-STA-12 are similar to those of a

(50) Zecchina, A.; Otero Arean, C.; Turnes Palomino, G.; Geobaldo, F.; Lamberti, C.; Spoto, G.; Bordiga, S. *Phys. Chem. Chem. Phys.* **1999**, *1*, 1649–1657.

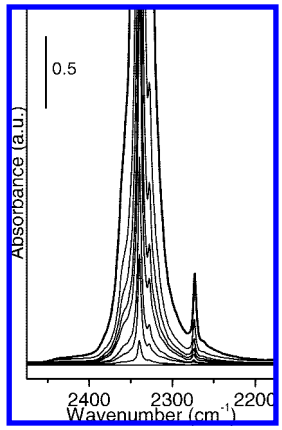

Figure 17. Background-subtracted IR spectra of increasing coverage of CO_2 at 300 K on Ni-STA-12.

NaY zeolite,[51] and this confirms that Ni-STA-12 contains some relatively polar centers. The enthalpies are greater in magnitude than the -22 kJ mol^{-1} obtained for the carboxylate-based MOF MIL-47,[52] which has pores of similar size but contains no coordinatively unsaturated metal sites. Note that greater initial heats of adsorption have been observed with MOFs such as MIL-100 or MIL-101[53] which have coordinatively unsaturated sites.

Even without thermal activation, the partially dehydrated solid shows a capacity that approaches 4 mmol g^{-1} at 15 bar. However, while the initial adsorption enthalpies are of a similar value to those observed on the fully dehydrated sample (possibly suggesting some nickel sites could have been dehydrated), they decrease rapidly with increasing coverage. This highlights how the chemisorbed water shields the nickel cation sites, and that the CO_2 interacts with hydroxyl groups and/or the organic groups of the framework less strongly than with dehydrated nickel sites.

Insight on the nature of the adducts formed with CO_2 has been obtained from infrared spectra collected at room temperature on a fully dehydrated sample in the 0−9 mbar pressure range. Due to the very high extinction coefficient of the ν_3 CO_2 mode (asymmetric O−C−O stretch), the spectra quickly go off-scale. The coordination vacancies of Ni sites of STA-12 are readily saturated by CO_2, forming linear adducts that show an intense absorption at 2339 cm^{-1} (background-subtracted spectra are reported in Figure 17). A red shift with respect to the gas phase (2349 cm^{-1}) has been observed previously in the case of HKUST-1[1] and can be explained in this case by considering the interaction of CO_2 with the full NiO_4N unit, rather than the interaction with bare Ni(II) that should give blue shifts as observed with oxides and zeolites.[1]

For methane the initial enthalpy of adsorption is -14 to -16 kJ mol^{-1}, increasing in magnitude to around -20 kJ mol^{-1} at higher pressures and uptakes as sorbate−sorbate interactions become important. The results indicate that the amount of carbon dioxide taken up by Ni-STA-12 is around 10 times that of methane at 1 bar, a ratio higher than that observed for adsorption on other large-pore MOF materials, such as MIL-100 and MIL-101.[12] The ratio is closer to that observed for cationic zeolites and suggests that good selectivities in adsorption from gas mixtures may be possible.

Summary and Conclusions

As prepared, the large-pore metal phosphonate Ni-STA-12 contains physisorbed water molecules within the pores and chemisorbed molecules coordinated to the nickel cations of the nickel phosphonate framework, which adopt octahedral NiO_5N coordination (unit composition $Ni_{18}(H_2O)_{18}L_9 \cdot 54H_2O$). Structure solution at 100 K reveals that all of these water molecules together form a well-ordered, tetrahedrally coordinated, hydrogen-bonded network, reminiscent of hexagonal ice. The hydrogen-bonded network is also evident from room-temperature infrared spectroscopy of the hydrated phase.

The dehydration and rehydration behavior of Ni-STA-12 has been studied by both laboratory and synchrotron X-ray powder diffraction, and also by infrared spectroscopy. The rehydration has been found to be rapid and fully reversible. Dehydration takes place in two main steps: physisorbed water is lost by gentle heating under vacuum to give the rhombohedral $Ni_{18}(H_2O)_{18}L_9$, while chemisorbed water is lost completely above 373 K to give a triclinic phase, unit cell composition Ni_6L_3. High-resolution thermogravimetric analysis indicates that the chemisorbed water is lost in two steps, in the weight ratio 2:1, and parallel XRD studies indicate an intermediate dehydrated phase with triclinic symmetry, which has the unit cell composition $Ni_6(H_2O)_2L_3$. It has been possible to solve the structure of the fully dehydrated Ni-STA-12 from high-resolution XRD data, which shows that the structure has adapted to water loss by movement of the phosphonate tetrahedra and transformation of the nickel coordination to NiO_4N polyhedra, leaving one in three of the phosphonate groups with a P═O bond projecting into the pores. Comparison of hydrated and fully dehydrated structures indicates that this is the result of two out of three phosphonate groups rotating and adopting additional coordination to nickel cations. Vibrational and electronic spectroscopies follow the remarkable structural changes that occur upon complete dehydration and confirm the reversibility of the process. IR data suggest that the first water molecules added to the dehydrated phase coordinate the nickel cations and hydrogen-bond to the phosphonate oxygen atoms that move to project into the pores, leaving free hydroxyl groups, thought to be attached to the nickel cations. Adding further water results in adsorption and hydrogen-bonding to the free hydroxyls, giving a fully H-bonded array.

The dehydrated phases of Ni-STA-12 present a range of adsorption sites to adsorbate molecules that are different from those observed in other MOFs or in zeolites. For the fully dehydrated material, these include incompletely coordinated nickel cation sites (with three crystallographically distinct sites) and P═O groups on one in three phosphonates, as well as sites on the organic linkers. In the partially dehydrated form, free and hydrogen-bonded hydroxyl groups are present instead. Both types of samples exhibit permanent porosity, for example in the adsorption of carbon dioxide, but higher heats and adsorption capacities (6 mmol g^{-1}) are observed on the fully dehydrated solid.

Adsorption of H_2 on the fully dehydrated solid at 77 K shows strong adsorption of 2 mmol g^{-1}, whereas adsorption of CO at the same temperature shows strong interactions up to 5 mmol g^{-1}, suggesting the structure can adjust to accommodate the CO at all nickel sites (as observed for water and acetonitrile),

(51) Maurin, G.; Llewellyn, P. L.; Bell, R. G. *J. Phys. Chem. B* **2005**, *109*, 16084–16091.
(52) Bourrelly, S.; Llewellyn, P. L.; Serre, C.; Millange, F.; Loiseau, T.; Férey, G. *J. Am. Chem. Soc.* **2005**, *127*, 13519–13521.
(53) Llewellyn, P. L.; Bourrelly, S.; Serre, C.; Vimont, A.; Daturi, M.; Hamon, L.; De Weireld, G.; Chang, J.-S.; Hong, D.-Y.; Hwang, Y. K.; Jhung, S. H.; Férey, G. *Langmuir* **2008**, *24*, 7245–7250.

whereas the adsorption of H_2 at 77 K occurs only on the most accessible nickel cation sites.

Adsorption and calorimetry of CO_2 and CH_4 on fully dehydrated Ni-STA-12 up to 1 bar and at 304 K show that more CO_2 is taken up than methane by a factor of 10, which is higher than that observed for the MOFs MIL-100 and MIL-101, although it is lower than for cationic zeolites. The adsorption sites have been investigated further by IR spectroscopy of adsorbed probe molecules H_2, CO, and CO_2, which have been dosed sequentially onto dehydrated Ni-STA-12. The different types of nickel cations act as Lewis acid sites with different strengths of interaction, depending on their local geometry, and there is also evidence that the P═O groups interact weakly, giving rise to red shifts of the carbon monoxide stretching band. This unusual array of adsorption sites is expected to show unusual adsorption selectivities for separation and purification. In addition, it may be that STA-12 can show characteristic catalytic activities, particularly given that STA-12 can be prepared in which Fe(II) and Co(II) can take the place of Ni(II) in the framework.

Acknowledgment. S.R.M., P.A.W., G.F., S. Bourrelly, and P.L.L. gratefully acknowledge funding from the EC STREP program 'DeSANNS' (SES6-CT-2005-020133). G.M.P. and S. Bordiga acknowledge support from the EC NoE 'IDECAT'.

Supporting Information Available: Crystallographic data, including CIF files for Ni-STA-12 (hydrated and dehydrated at 323 and 523 K); Rietveld refinement and atomic coordinate data, with modeled hydrogen positions; infrared spectra of methanol and deuterioacetonitrile adsorbed on Ni-STA-12; and nitrogen adsorption isotherm and differential heats of calorimetry measured at 77 K. This material is available free of charge via the Internet at http://pubs.acs.org.

JA804936Z